Analytical solution to a fracture problem in a tough layered structure

Yukari Hamamoto and Ko Okumura
Department of Physics, Graduate School of Humanities and Sciences, Ochanomizu University, 2-1-1, Otsuka, Bunkyo-ku, Tokyo 112-8610, Japan

(Received 14 January 2008; revised manuscript received 26 June 2008; published 22 August 2008)

Nacre causes the shining beauty of pearl due to its remarkable layered structure, which is also strong. We reconsider a simplified layered model of nacre proposed previously [Okumura and de Gennes, Eur. Phys. J. E **4**, 121 (2001)] and obtain an analytical solution to a fundamental crack problem. The result asserts that the fracture toughness is enhanced due to a large displacement around the crack tip (even if the crack-tip stress is not reduced). The derivation offers ideas for solving a number of boundary problems for partial differential equations important in many fields.

DOI: 10.1103/PhysRevE.78.026118 PACS number(s): 46.50.+a, 87.85.jc, 62.25.Mn, 81.07.Pr

Nacre is not only beautiful but also strong. A prominent feature of this substance is a layered structure at submicrometer scale. This structure is the origin of the shining beauty of pearl, and it is known to possess a remarkable toughness [1,2] which has been studied over many years [3–14].

One important factor governing the strength of a material is the *stress concentration* around ubiquitous small cracks in materials: around a crack tip the stress is enhanced, which breaks the bonds to initiate failure. One can feel this on the macroscopic level, just with a piece of paper: the sheet is actually rather strong if one tries to break it by applying tensile force with the hands, but it easily breaks if one introduces a cut (i.e., crack) by a sharp knife in the middle in the direction perpendicular to the tensile direction.

Among many ideas on the toughening mechanism of nacre, the possibility of reduction of such stress enhancement around the tip is suggested [5] by use of a simplified elastic model mimicking the structure and by consideration of a semi-infinite crack in the middle of an infinitely long plate of width $2L$ [Fig. 1(a)], which allows an analytical solution. However, the analytical solution to the more basic crack problem of a small *finite* line crack in a large plate has not been available [Fig. 1(b)]. In this study, we solve this finite-crack problem and show that, even if the crack-tip stress is not reduced, a strong displacement around the crack tip alone can increase the fracture toughness. The fundamental result obtained here is useful not only to understand the physics of strength of composite materials and to develop strong structured materials in industry, but also to offer ideas to solve the two-dimensional boundary problem for partial differential equations such as the Laplace equation important in many fields.

In the model, hard layers (thickness d_h and Young modulus E_h) are glued together by soft layers (thicknesses d_s and Young modulus E_s) as in Fig. 1 where the period of the stripe, d, is defined as $d=d_s+d_h$. We introduce small parameters ε_E and ε_d:

$$E_s=\varepsilon_E E_h,\quad d_s=\varepsilon_d d_h. \tag{1}$$

We require the following properties, which are important characteristics of our model:

$$\varepsilon \equiv \varepsilon_E d/d_s \cong \varepsilon_E/\varepsilon_d \ll 1. \tag{2}$$

Nacre may be modeled typically by $\varepsilon_E \cong 1/5000$ and $\varepsilon_d \cong 1/100$, where $\varepsilon \cong 1/50$.

In our previous paper [5], we showed that, for a line crack running in the x direction under the plane strain condition (thick plate), as in Figs. 1(a) and 1(b), the elastic energy per unit volume of the model can be reduced to

$$f=\frac{E_h}{2(1-\nu^2)}\left(\frac{\partial u_y}{\partial y}\right)^2+\frac{E_0}{4(1+\nu)}\left(\frac{\partial u_y}{\partial x}\right)^2 \tag{3}$$

with the formal relations $\partial_y \sim \sqrt{\varepsilon}\partial_x$ and $u_x \sim \sqrt{\varepsilon} u_y$, if we keep only the leading-order contributions $[\sim \varepsilon E_h(\partial_x u_y)^2]$. Here, u_i and ν are the displacement field and Poisson's ratio, respectively. The dominant component of stress derived from $\sigma_{ij}=\partial f/\partial e_{ij}$ is $\sigma_{yy}\sim\varepsilon^{1/2}$ while $\sigma_{xx}\sim\varepsilon^{3/2}$ and $\sigma_{xy}\sim\varepsilon$.

At equilibrium, by minimizing the volume integral over x and y of Eq. (3) with respect to u_y, we obtain the following reduced Laplace equation for the dominant displacement field u_y:

$$\left(\frac{\partial^2}{\partial \hat{x}^2}+\frac{\partial^2}{\partial y^2}\right)u_y=0, \tag{4}$$

where a reduced x coordinate has been introduced:

$$\hat{x}\equiv x/\sqrt{\epsilon}\quad \text{with } \epsilon=\varepsilon(1-\nu)/2. \tag{5}$$

As announced, we consider a finite line crack of length $2a$ in Fig. 1(b), for which the following boundary conditions are appropriate in the upper half plane $(y>0)$:

$$u_y=\begin{cases}u_0 & \text{at } y=L,\\ 0 & \text{for } y=0,\ x<-a \text{ or } x>a,\end{cases}$$

$$\frac{\partial u_y}{\partial y}=0\quad \text{for } y=0,\ -a<x<a. \tag{6}$$

Note that the original field u_y on the whole xy plane has a discontinuous jump at the crack surface ($-a<x<a$, $y=0$): u_y is positive for $y=0^+$ but negative for $y=0^-$.

To overcome the discontinuous jump at the crack surface, we consider an auxiliary field on the whole xy plane defined as

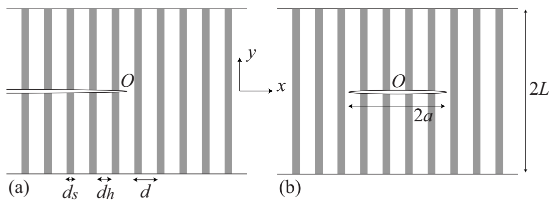

FIG. 1. Layered structure with a semi-infinite (a) and a finite (b) crack. In (a) and (b), the origin O of the xy coordinate is placed at the crack tip and at the middle point of the crack, respectively.

$$u \equiv \begin{cases} u_y, & y>0, \\ -u_y, & y<0. \end{cases} \tag{7}$$

By introducing this auxiliary field u, which is always positive and has no discontinuous jump at the crack surface, the original Cauchy boundary problem [both u_y and its derivative appear in boundary conditions as in Eq. (6)] is changed into a simpler Dirichlet boundary problem (u_y is always given at the boundary):

$$u = \begin{cases} u_0 & \text{at } y = \pm L, \\ 0 & \text{for } y=0,\ x<-a \text{ and } x<a. \end{cases} \tag{8}$$

A solution of the Laplace equation on the $(\hat{x},y)$ plane, u, satisfying Eq. (8), can be obtained by finding the conformal mapping from $z=\hat{x}+iy$ to $w=f(z)$ where Im w meets requirements specified by Eq. (8); we obtain

$$u_y = \mathrm{Im}\, w \quad \text{for } y>0, \tag{9}$$

because Im w of an analytic function w satisfies the Laplace equation. This implies, for $y>0$,

$$\sigma_{yy} = E\, \mathrm{Re}\, \frac{dw}{dz} \quad \text{with } E \equiv \frac{E_h}{1-\nu^2}. \tag{10}$$

The desired analytic function $w=f(z)$ can be found by introducing another complex plane ζ in order to consider a quasi-Schwarz-Christoffel transformation from $\zeta=\xi+i\eta$ to $z=\hat{x}+iy$ where

$$\frac{dz}{d\zeta} = k\frac{\zeta^2-1}{(\zeta+m)(\zeta-p)(\zeta-q)}, \tag{11}$$

with positive real numbers m, p, and q.

TABLE I. Arguments of complex variables for ζ on the real axis with Im $\zeta=0^+$.

	$\zeta<0$	$0<\zeta<p$	$p<\zeta<q$	$q<\zeta$
$\arg(\zeta)$	π	0	0	0
$\arg(\zeta-p)$	π	π	0	0
$\arg(q-\zeta)$	0	0	0	$-\pi$
$\arg(\frac{\zeta}{(\zeta-p)(q-\zeta)})$	0	$-\pi$	0	π
$2\arg(\frac{\zeta-p}{\zeta})$	0	2π	0	0

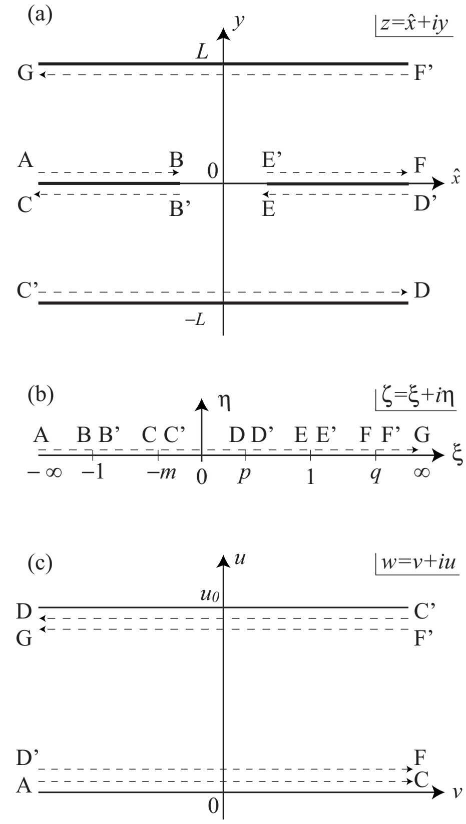

FIG. 2. Paths from A to G on the z (a) and w (c) planes corresponding to the path from A to G on the ζ plane (b). Real parts of the points D, D', F, F' in (a) and C, C', F, F' in (c) are ∞ and those of A, C, C', G in (a) and A, D, D', G in (c) are $-\infty$.

This transformation is examined in some detail to make the subsequent arguments understandable. Let us move ζ from $-\infty+i0^+$ to $+\infty+i0^+$ on the real axis of ζ (in the upper plane) passing through the intermediate points $\zeta=-1$, $-m,p,1,q$ [see Fig. 2(b)] and define the range of the principal value of the argument $\arg(Z)$ of a complex variable Z to be $-\pi<\arg(Z)\leqslant\pi$: if Z is on the real axis, with Re$[Z]$ positive, $\arg(Z)=0$, but, with Re$[Z]$ negative, $\arg(Z)=\pi$ and $-\pi$ when Im$[Z]$ is 0^+ and -0^+, respectively. Note that under this convention, the relation $\log(1/Z)=-\log Z$ is correct, but, in general, the relation

$$\log(z_1 z_2) = \log(z_1) + \log(z_2) \tag{12}$$

is correct only when

$$-\pi < \arg(z_1), \arg(z_1), \arg(z_1 z_2) \leqslant \pi. \tag{13}$$

Note that "log" stands for the natural logarithmic function. If the sum $\arg(z_1)+\arg(z_1)$ is not in the above range, we have to add on the right-hand side of Eq. (12) $2\pi i$ or $-2\pi i$ so that the imaginary part of both sides of Eq. (12) becomes equal. For example, we obtain

$$\log(-z_1) = \begin{cases} i\pi + \log(z_1), & -\pi < \arg(z_1) \leqslant 0, \\ -i\pi + \log(z_1), & 0 < \arg(z_1) \leqslant \pi. \end{cases} \tag{14}$$

Let us go back to the above movement on the real axis in the ζ plane in Fig. 2(b), from A to G. During this movement, for an increase in ζ, $\mathrm{Re}[d\zeta]$ is positive and $\mathrm{Im}[d\zeta]=0^{+}$, i.e., $\arg(d\zeta)=0$, so that

$$\arg(dz)=\arg(dz)-\arg(d\zeta)=\arg(dz/d\zeta) \tag{15}$$

$$=\arg(k)+\arg(\zeta+1)-\cdots-\arg(\zeta-q). \tag{16}$$

The first equality holds because of $\arg(d\zeta)=0$ and the third follows from Eq. (11). From Eq. (16), we see that, for example, when we pass $\zeta=q$ from the left to the right, $\arg(\zeta-q)$ changes from π to 0, with the other terms in the last line in Eq. (16) unchanged; $\arg(dz)$ is constant when ζ approaches q from the left, is changed by π at $\zeta=q$, and is constant again when ζ goes away from q: z could move on a straight line ($\zeta<q$) and jump to another straight line ($\zeta>q$) with a rotation by the angle π at $\zeta=q$, with z following the path $E'\to F\to F'\to G$ in Fig. 2(a). Indeed, we can choose unknowns (k,m,p,q plus an integration constant k') in such a way that the movement of ζ (with $\mathrm{Im}\,\zeta=0^{+}$), $A\to B\cdots\to G$ in Fig. 2(b) is mapped to the movement $A\to\cdots\to G$ in Fig. 2(a) on the z plane. For this purpose, we integrate Eq. (11) and determine the unknowns by the following conditions: (I) z has to make specified jumps at passages C-C', D-D', and F-F' (e.g., at the passage $F\to F'$, z jumps from ∞ to $\infty+iL$) and (II) z should be $\pm\hat{a}$ when $\zeta=\pm1$ where $\hat{a}\equiv a/\sqrt{\epsilon}$. From I and II, we find

$$z=\frac{L}{\pi}\log\frac{(q-p)\zeta}{(\zeta-p)(q-\zeta)} \tag{17}$$

with

$$m=0,\quad p=\tanh\frac{\pi\hat{a}}{2L}<1,\quad q=\coth\frac{\pi\hat{a}}{2L}>1. \tag{18}$$

Indeed, we can easily confirm that the transformation given in Eq. (17) satisfies the above required conditions. From Table I, for example, at the passages $C\to C'$ ($\zeta=0$) and $D\to D'$ ($\zeta=p$),

$$\mathrm{Im}\,z=\frac{L}{\pi}\arg\left(\frac{\zeta}{(\zeta-p)(q-\zeta)}\right) \tag{19}$$

jumps by the amount $-L$ and L, respectively. At $\zeta=\pm1$, the right-hand side of Eq. (17) reduces to $\pm\hat{a}$ by noting the relation

$$\frac{1}{q-p}=\cosh\frac{\pi\hat{a}}{2L}\sinh\frac{\pi\hat{a}}{2L}. \tag{20}$$

Next we find a transformation $\zeta\leftrightarrow w$ (appropriate for the desired transformation $z\leftrightarrow w$), not in the form of the Schwarz-Christoffel transformation, by noting that, when ζ is on the real axis (with $\mathrm{Im}\,\zeta=0^{+}$), $\mathrm{Im}\,W=u_1$ for $\zeta<\xi_0$ while $\mathrm{Im}\,W=u_2$ for $\zeta>\xi_0$, in a transformation $\zeta\leftrightarrow W$,

$$W(\zeta_0,u_1,u_2)=iu_2+\frac{u_1-u_2}{\pi}\log(\zeta-\xi_0). \tag{21}$$

The boundary condition in Eq. (8) states that, along the paths $A\to B\to C$ and $D'\to E\to F$ in Fig. 2(a), $u=\mathrm{Im}\,w$ should be zero while this should be u_0 on the paths $C'\to D$ and $F'\to G$. This results in the following condition for the transformation $\zeta\leftrightarrow w$ ($m=0$), from Fig. 2(b): on the real axis of ζ (with $\mathrm{Im}\,\zeta=0^{+}$), $\mathrm{Im}\,w=0$ for $\zeta<-m$ and $p<\zeta<q$ while $\mathrm{Im}\,w=u_0$ for $-m<\zeta<p$ and $q<\zeta$. This condition is satisfied for

TABLE II. Imaginary part of functions for ζ on the real axis with $\mathrm{Im}\,\zeta=0^{+}$.

	$\zeta<0$	$0<\zeta<p$	$p<\zeta<q$	$q<\zeta$
$\mathrm{Im}\,W\,(0,0,u_0)$	0	u_0	u_0	u_0
$\mathrm{Im}\,W\,(p,0,-u_0)$	0	0	$-u_0$	$-u_0$
$\mathrm{Im}\,W\,(q,0,u_0)$	0	0	0	u_0
$\mathrm{Im}\,w$	0	u_0	0	u_0

$$w=W(0,0,u_0)+W(p,0,-u_0)+W(q,0,u_0). \tag{22}$$

Indeed we can check this by Table II.

Equation (22) can be manipulated with the aid of Eq. (12):

$$w=\frac{u_0}{L}z+\frac{2u_0}{\pi}\log\frac{\zeta-p}{\zeta}. \tag{23}$$

Here, z is given by Eq. (17). As a matter of fact, we can confirm that w given in Eq. (23) as a function of ζ moves on the path A to G in Fig. 2(c) as ζ goes along the path $A-G$ in Fig. 2(b): we can check that $\mathrm{Im}\,w=0$ at $\zeta=1+i0^{+}$ and that w makes necessary jumps at intermediate points [e.g., at the passage C to C' ($\zeta=0$), $\mathrm{Im}\,w$ jumps by the amount iu_0], with the aid of Table I, by noting the relation

$$\mathrm{Im}\,w=\frac{u_0}{\pi}\left[\arg\left(\frac{\zeta}{(\zeta-p)(q-\zeta)}\right)+2\arg\left(\frac{\zeta-p}{\zeta}\right)\right] \tag{24}$$

obtained from Eqs. (19) and (23). Thus, Eq. (23) guarantees the movement on the w plane from A to G along straight lines with rotations by the angle π at C, D, and G [Fig. 2(c)] when ζ moves on the real axis from A to G [Fig. 2(b)], as can be checked by using a relation similar to Eq. (16). We stress here that the transformation in Eq. (23) is not the Schwarz-Christoffel transformation: the derivative of Eq. (23),

$$\frac{dw}{d\zeta}=\frac{(\zeta-\zeta_{+})(\zeta-\zeta_{-})}{\zeta(\zeta-p)(\zeta-q)}, \tag{25}$$

with points $\zeta_{\pm}=p\pm i\sqrt{1-p^2}$ located off the real axis.

Finally, we derive the transformation $z\leftrightarrow w$. From Eq. (17), we obtain

$$\zeta=\phi(z)+\varphi(z) \tag{26}$$

[the reason we have selected the plus sign in front of $\varphi(z)$ can be seen in Eq. (36) below], where

$$2\phi(z)\equiv(p+q)-(q-p)e^{-\pi z/L}, \tag{27}$$

$$\varphi(z)\equiv[\phi(z)^2-1]^{1/2}. \tag{28}$$

Equation (23) with Eqs. (26)–(28) completely defines the desired transformation $z\leftrightarrow w$.

From this Eq. (23), the displacement field and stress field are analytically obtained through Eqs. (9) and (10):

$$u_y = \frac{u_0}{L}y + \frac{2u_0}{\pi}\arctan\left(\frac{\mathrm{Im}\left(1-\dfrac{p}{\phi(z)+\varphi(z)}\right)}{\mathrm{Re}\left(1-\dfrac{p}{\phi(z)+\varphi(z)}\right)}\right), \quad (29)$$

$$\sigma_{yy} = \sigma_0\left[1+\mathrm{Re}\left(\frac{p(p+q-2\phi(z))}{\varphi(z)[\phi(z)-p+\varphi(z)]}\right)\right], \quad (30)$$

where σ_0 is a measure of the remote stress,

$$\sigma_0 \equiv Eu_0/L. \quad (31)$$

The crack shape and stress concentration around the crack tip are examined by putting $z=\hat{a}-\hat{r}+i0^+$ in Eq. (29) and $z=\hat{a}+\hat{r}+i0^+$ in Eq. (30), where $\hat{r}\equiv r/\sqrt{\epsilon}$, so that r represents the distance from the crack tip. For small Δ, we have

$$\phi(\hat{a}+\Delta) \simeq 1 + \frac{\pi(p+q-2)}{2L}\Delta, \quad (32)$$

$$\varphi(\hat{a}+\Delta) \simeq [\pi(p+q-2)\Delta/L]^{1/2}, \quad (33)$$

where

$$p+q-2 = (q-p)e^{-\pi\hat{a}/L} > 0. \quad (34)$$

Thus, at $z=\hat{a}-\hat{r}+i0^+$, we have

$$\frac{1}{\phi(z)+\varphi(z)} = 1 - i[\pi(p+q-2)\hat{r}/L]^{1/2} \quad (35)$$

and

$$u_y = \frac{2u_0}{\pi}\frac{p[\pi(p+q-2)\hat{r}/L]^{1/2}}{1-p} = 2\kappa u_0\sqrt{\frac{\hat{r}}{\pi L}} \quad (36)$$

[the wrong sign in Eq. (26) would give the wrong sign for this expression]. At $z=\hat{a}+\hat{r}+i0^+$, we have

$$\sigma_{yy} \simeq \sigma_0\,\mathrm{Re}\left(\frac{p(p+q-2)}{\varphi(z)(1-p)}\right) = \kappa\sigma_0\sqrt{\frac{L}{\pi\hat{r}}}, \quad (37)$$

where

$$\kappa \equiv \frac{p\sqrt{p+q-2}}{1-p} = \frac{e^{\pi\hat{a}/L}-1}{\sqrt{e^{2\pi\hat{a}/L}-1}}. \quad (38)$$

We consider the limit $L \ll \hat{a}$, which includes the case $L \simeq a$, for which we have $\kappa \simeq 1$. In this limit, for $y=0^+$, the displacement at $x=a-r$ and the stress at $x=a+r$ are given by

$$u_y = 2\epsilon^{-1/4}\frac{K_L\sqrt{r}}{E}, \quad \sigma_{yy} = \epsilon^{1/4}\frac{K_L}{\sqrt{r}} \quad \text{with } K_L \equiv \sigma_0\sqrt{L/\pi}. \quad (39)$$

The tip displacement is enhanced by a factor $\epsilon^{-1/4}$ while the tip stress concentration is reduced by a factor $\epsilon^{1/4}$, compared with a monolithic material of the same size with the same crack.

We next consider the limit $L \gg \hat{a}$, corresponding to an infinite plate as in the Griffith problem, where $\kappa \simeq \sqrt{\pi\hat{a}/2L}$. In this limit, for $y=0^+$, the displacement at $x=a-r$ and the stress at $x=a+r$ are given by

$$u_y = \epsilon^{-1/2}\frac{2K_a\sqrt{r}}{E}, \quad \sigma_{yy} = \frac{K_a}{\sqrt{r}} \quad \text{with } K_a \equiv \sigma_0\sqrt{a/2}. \quad (40)$$

Tip displacement is enhanced by a larger factor $\epsilon^{-1/2}$ while the tip-stress singularity is the same as that of the pure material of the same size with the same crack [see Eq. (39)].

As a matter of fact, most of the scaling structures in expressions obtained from the present analytical solution can be reproducible from simple scaling arguments, which require a separate presentation [15], where we show a useful general formula on the fracture toughness. Here, the fracture toughness is defined in a standard way [16] as the value of the energy release rate, G, at the critical of failure where G is given by $G=-d\Pi/da$ and Π is the elastic potential energy per unit width of the crack front. In the general formula, the fracture toughness is enhanced by

$$\lambda = (\lambda_u/\lambda_\sigma)(d/a_0), \quad (41)$$

where λ_u, λ_σ, and a_0 are the tip-displacement enhancement factor, the tip-stress reduction factor, and the typical size of Griffith flaws in the hard sheets: the tip-displacement enhancement ($\lambda_u \geq 1$) and the tip-stress reduction ($\lambda_\sigma \leq 1$) are two independent origins of the fracture toughness. In the above two different limits of $L \ll \hat{a}$ and $L \gg \hat{a}$, we obtained different sets of factors $(\lambda_u,\lambda_\sigma)=(\epsilon^{-1/4},\epsilon^{1/4})$ and $(\epsilon^{-1/2},1)$, respectively [see Eqs. (39) and (40)], so that the physical origins of the toughening are different: in the limit $L \ll \hat{a}$, similar to the result in [5], both enhancement of tip displacement and reduction of tip-stress concentration contribute, while only a stronger tip-displacement enhancement plays a role in the limit $L \gg \hat{a}$. However, the enhancement factor of the fracture toughness λ given in Eq. (41) is the same in the two different limits of $L \ll \hat{a}$ and $L \gg \hat{a}$: $\lambda=\epsilon^{-1/2}(d/a_0)$. From this robust universal relation, we could deduce the reason of ubiquitousness of strong nanostructured soft-hard composites in nature [15].

The physical reasons for the above deformation enhancement and reduction of the stress concentration due to the layered structure can be understood (with the help of the physical pictures obtained from the scaling arguments) [15]: for example, in a discrete model where soft and hard layers are treated as blocks (distinguishing stress and strain in two different soft and hard phases on a scale smaller than d), displacements in soft layers are significant (this is partially confirmed in simulation [17]), which contributes to the displacement enhancement in the present continuum model applicable on scales larger than the block sizes. In conclusion, we have analytically solved the finite-crack problem for a layered structure mimicking nacre, i.e., a boundary problem for the Laplace equation on a reduced plane $(\hat{x},y)$. This was carried out by replacing a Cauchy problem for a singular field u_y with a Dirichlet problem for a regular auxiliary field u and by finding an appropriate conformal mapping $z \leftrightarrow w$

via another complex plane ζ where a non-Schwarz-Christoffel transformation was involved. Technically, the derivation will help in solving certain boundary problems in many different fields. Physically, the result clarifies two origins of strength of the special layered structure of macroscopic size: (i) a reduced crack-tip stress and (ii) a strong displacement around the crack tip. In particular, even without (i), due to (ii) alone, the fracture toughness can be increased significantly.

This work is supported by KAKENHI from MEXT, Japan.

[1] J. D. Currey, Proc. R. Soc. London, Ser. B **196**, 443 (1977).

[2] A. P. Jackson, J. F. V. Vincent, and R. M. Turner, Proc. R. Soc. London, Ser. B **234**, 415 (1988).

[3] M. Sarikaya and I. A. Aksay, *Biomimetics: Design and Processing of Materials* (AIP, New York, 1995).

[4] M. P. Rao, A. J. Sanchez-Herencia, G. E. Beltz, R. M. McMeeking, and F. F. Lange, Science **286**, 102 (1999).

[5] K. Okumura and P. G. de Gennes, Eur. Phys. J. E **4**, 121 (2001); P. G. de Gennes and K. Okumura, C. R. Acad. Sci., Ser IV: Phys., Astrophys. **1**, 257 (2000).

[6] K. Okumura, Eur. Phys. J. E **7**, 303 (2002); Europhys. Lett. **63**, 701 (2003); J. Phys.: Condens. Matter **17**, S2879 (2005); K. Okumura, Europhys. Lett. **67**, 470 (2004).

[7] A. G. Evans, Z. Suo, R. Z. Wang, I. A. Aksay, M. Y. He, and J. W. Hutchinson, J. Mater. Res. **16**, 2475 (2001).

[8] D. R. Kattii, K. S. Katti, J. Sopp, and M. Sarikaya, Comput. Theor. Polym. Sci. **11**, 397 (2001).

[9] H. J. Gao, B. H. Ji, I. L. Jager, E. Artz, and P. Fratzl, Proc. Natl. Acad. Sci. U.S.A. **100**, 5597 (2003).

[10] F. Song and Y. L. Bai, J. Mater. Res. **18**, 1741 (2003).

[11] P. Franzl, H. S. Gupta, E. P. Paschalis, and P. Roschger, J. Mater. Chem. **14**, 2115 (2004).

[12] B. Ji and H. Gao, J. Mech. Phys. Solids **52**, 1963 (2004).

[13] Phani Kumar V. V. Nukala and S. Šimunović, Phys. Rev. E **72**, 041919 (2005).

[14] F. Barthelat, C.-M. Li, C. Comi, and H. D. Espinosa, J. Mater. Res. **21**, 1977 (2006).

[15] K. Okumura (unpublished).

[16] T. L. Anderson, *Fracture Mechanics-Fundamentals and Applications* (CRC Press, Boca Raton, FL, 1991).

[17] S. Nakagawa and K. Okumura, J. Phys. Soc. Jpn. **76**, 114801 (2007); Y. Aoyanagi and K. Okumura (unpublished); (unpublished).